Topology-dependent giant-atom interaction in a topological waveguide QED system

Da-Wei Wang,[1] Chengsong Zhao,[1] Ye-Ting Yan,[1] Junya Yang,[1] Zhihai Wang,[2] and Ling Zhou[1,*]

[1]*School of Physics, Dalian University of Technology, Dalian 116024, People's Republic of China*

[2]*Center for Quantum Sciences and School of Physics, Northeast Normal University, Changchun 130024, People's Republic of China*

(Received 26 January 2024; accepted 15 May 2024; published 31 May 2024)

We investigate topology-dependent giant-atom–photon bound states in a giant-atom coupled topological waveguide system and find that the bound states can induce topology-dependent dipole-dipole interactions between giant atoms. For bridged giant atoms, when the waveguide is in the topological phase, there is no interaction between them and the atom-atom interaction can only survive in the trivial phase. Conversely, for separated giant atoms, they interact with each other only in the topological phase rather than in the trivial phase. The characteristics of these two cases provide us a way to model pure nearest-neighbor interactions and double chains, respectively. Our work may promote the application of topological physics in quantum information processes and quantum simulations.

DOI: 10.1103/PhysRevA.109.053720

I. INTRODUCTION

In conventional waveguide-QED systems [1,2], atoms are considered as pointlike objects if the wavelength of the atoms is much smaller than the wavelength of the coupling field, which is also known as the dipole approximation [3]. Recently, a new model of giant atoms has been developed in artificial atomic systems in which the giant atom can simultaneously couple with the waveguide at different points, for example, the superconducting quantum qubits can be considered as giant atoms by employing the small atom coupling to a waveguide at multiple nodes [4]; the coupling of giant atoms to surface acoustic waves and to microwave waveguides has also been reported [5–7]. A theoretical scheme for the realization of giant atoms in dynamic state-dependent optical lattices using ultracold atoms has been proposed [8]. In addition, the giant-atom physics has also been extended to giant molecules [9,10] and giant spin ensembles [11,12]. Compared to pointlike atoms, the giant atoms can be conjoined to the waveguide by multiple coupling points, which leads to many peculiar phenomena due to the interference and time-delay effects between the coupling points such as frequency-dependent decay rates and Lamb shifts [13], waveguide-mediated decoherence-free interaction [14–16], chiral phenomena [10,17–20], generation of two-giant-atom entanglement [21,22], oscillating bound states [23–25], and non-Markovian effects [26–28].

In recent years, topological photonics have received a great deal of attention in quantum physics because of their many interesting features, including robustness to local decoherence processes and potential applications in quantum information [29–32]. The topological waveguide (TW) described by the Su-Schrieffer-Heeger (SSH) model has been realized in a superconducting circuit [33,34] and photonic waveguide [35,36]. Meanwhile, atoms coupled with a TW present new opportunities to study single-excitation dynamics such as topologically protected states and photon-mediated interactions between atoms [34,37–41]. In particular, several unconventional quantum optical phenomena were predicted and realized when quantum emitters interact with a TW such as the emergence of chiral bound states, directional dipole-dipole interactions, and topologically dependent super- and subradiative states [42–45]. Many works have pointed out the importance of topology for quantum physics such as topologically protected atomic coherence [46], enhanced nonreciprocal scattering and photon absorption [47], and protected optomechanically induced transparency [48].

In conventional atom-photon bound-state theories, photons tend to be symmetrically localized around atoms and the overlapping of the wave functions of photon bound states around different atoms can cause the exchange of photons, which in turn induces the interaction between atoms [49–51]. Thus, by designing a special distribution of atom-photon bound states, the special interaction between atoms can be engineered. In this paper we consider the topological effects on the giant-atom–photon bound states in the giant-atom coupled TW system and show that the spatial distribution of the giant-atom–photon bound states exhibits a clear topological dependence. When multiple giant atoms are coupled within the band gap of the TW, due to the overlap of the bound-state wave functions, the effective dipole-dipole interactions between the giant atoms are generated by exchanging virtual photons, and the strength of the interactions depends on the degree of overlap between the bound states. Thus, topologically dependent bound states can induce topologically dependent dipole-dipole interactions between giant atoms. In the trivial phase, nearest-neighbor interaction between giant atoms can be obtained; in the topological phase, a double chain of the atoms can be realized. These characteristics are valuable in quantum information and quantum simulation.

*zhlhxn@dlut.edu.cn

 ©2024 American Physical Society

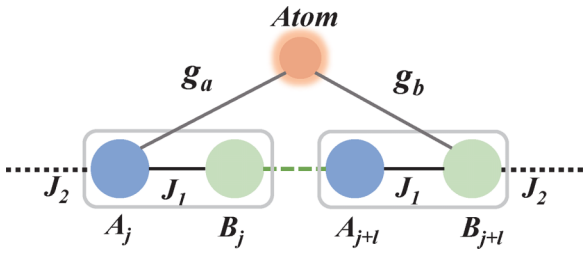

FIG. 1. Schematic diagram of a giant atom coupled to an SSH chain. Each cell of the SSH chain contains two sublattices A and B, with intercellular and extracellular coupling strengths of J_1 and J_2, respectively. The giant atoms can couple with the TW at cells j and $j+l$ with strengths of g_a and g_b, respectively.

II. MODEL

As shown in Fig. 1, we consider that the giant atoms with two coupling nodes couple to a SSH chain at cells j and $j+l$ with strengths of g_a and g_b, respectively. The distance between two coupling nodes of a single giant atom is l. Experimentally, the SSH chain has been realized in superconducting circuit systems, where each cell of the SSH chain can be mapped to the two LC resonators (microwave cavity). In addition, the intra- and intercellular couplings between neighboring resonators have been determined by the auxiliary capacitance and inductance [34]. Each cell contains two sublattices A and B with frequencies ω_a and intercellular and extracellular couplings with strengths J_1 and J_2, respectively. The total Hamiltonian of the system can be written as

$$H = H_0 + H_I + H_B, \tag{1}$$

with

$$\begin{aligned} H_0 &= \sum_{n=1}^{M} \Delta\sigma_n^\dagger\sigma_n, \\ H_I &= \sum_{n=1}^{M}[(g_a a_n^\dagger + g_b b_{n+l}^\dagger)\sigma_n + \text{H.c.}], \\ H_B &= \sum_{j=-N}^{N}(J_1 a_j^\dagger b_j + J_2 a_{j+1}^\dagger b_j + \text{H.c.}), \end{aligned} \tag{2}$$

where $a_n^\dagger$ ($b_n^\dagger$) and a_n (b_n) are the creation and annihilation operators for the microwave cavity, respectively; $\sigma_n = |g\rangle\langle e|$ is the spin operator representing the transition $|e\rangle \to |g\rangle$; H_0 denotes the free energy of the giant atom with the detuning $\Delta = \omega_0 - \omega_a$, where we use the center frequency of the SSH chain ω_a as the reference energy and ω_0 is the frequency of the giant atom; H_I represents the interaction between giant atoms and the SSH chain, where n denotes the position of the left coupling point of the giant atom corresponding to the cavity; and H_B is the Hamiltonian of the SSH chain. Hereafter, we set $J_1 = J(1-\delta)$ and $J_2 = J(1+\delta)$, with J as a unit. We consider the weak-coupling condition, i.e., $(g_a, g_b) \ll (J_1, J_2)$. Under this condition, we can first diagonalize the Hamiltonian H_B with periodic boundary condition and then H_B in the momentum space can be written as

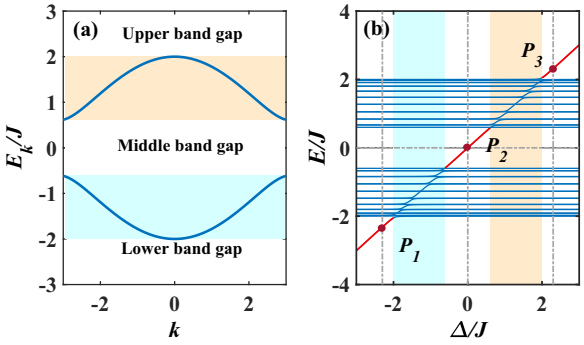

FIG. 2. (a) Variation of the energy dispersion of the SSH chain with k (dimensionless) in the first Brillouin zone. (b) Variation of the energy spectra with Δ for $\delta = 0.3$. The other parameters are $g_a = 0.1J$, $g_b = 0.1J$, $m = 10$, and $N = 20$.

$$\begin{aligned} H_B &= \sum_k (J_1 + J_2 e^{-ik}) a_k^\dagger b_k + (J_1 + J_2 e^{ik}) b_k^\dagger a_k \\ &= \sum_k \psi_k^\dagger H_B(k) \psi_k, \end{aligned} \tag{3}$$

where $\psi_k^\dagger = (a_k, b_k)$, $a_k = \frac{1}{\sqrt{N}}\sum_j a_j e^{-ikx_j}$, $b_k = \frac{1}{\sqrt{N}}\sum_j b_j e^{-ikx_j}$, and $H_B(k)$ is given by

$$H_B(k) = \begin{pmatrix} 0 & f(k) \\ f^*(k) & 0 \end{pmatrix}, \tag{4}$$

with $f(k) = J_1 + J_2 e^{-ik}$. The dispersion relation of the SSH model [energy spectrum of Eq. (4)] can be calculated as $E(k) = \pm\omega(k) = \pm\sqrt{J_1^2 + J_2^2 + 2J_1 J_2 \cos(k)}$. In Fig. 2(a) we plot $E(k)$ varying with k in the first Brillouin zone. It can be seen that the energy spectrum of the SSH model can be divided into two parts. One is the energy-band region, including the upper energy band (orange) and the lower energy band (cyan), where photons can propagate in the TW with velocity $v_g = \partial E(k)/\partial k$. The other region is the band gap region, where photons are forbidden to propagate. In the momentum space, the interaction Hamiltonian H_I becomes

$$H_I = \frac{1}{\sqrt{N}}\sum_{n=1}^{M}\sum_k \{e^{-ikx_n}[(g_a a_k^\dagger + g_b b_k^\dagger e^{-ilk})]\sigma_n + \text{H.c.}\}. \tag{5}$$

Given that the SSH model satisfies the chiral symmetry, we can diagonalize $H_B(k)$ as $H_B = \sum_k \omega(k)(\alpha_k^\dagger\alpha_k - \beta_k^\dagger\beta_k)$, where the relationship between the diagonalized bases (α_k, β_k) and (a_k, b_k) satisfies

$$\begin{pmatrix} a_k \\ b_k \end{pmatrix} = \frac{1}{\sqrt{2}}\begin{pmatrix} 1 & -1 \\ e^{-i\phi(k)} & e^{-i\phi(k)} \end{pmatrix}\begin{pmatrix} \alpha_k \\ \beta_k \end{pmatrix}. \tag{6}$$

Substituting Eq. (6) into Eq. (5), we obtain

$$H_I = \frac{1}{\sqrt{N}}\sum_{n=1}^{M}\sum_k \{[p(k)\alpha_k^\dagger + q(k)\beta_k^\dagger]e^{-ikx_n}\sigma_n + \text{H.c.}\}, \tag{7}$$

where $p(k) = \frac{1}{\sqrt{2}}(g_a + g_b e^{-ikl} e^{i\phi(k)})$ and $q(k) = \frac{1}{\sqrt{2}}(-g_a + g_b e^{-ikl} e^{i\phi(k)})$, with $\phi(k) = \arctan \frac{J_2 \sin(k)}{J_1 + J_2 \cos(k)}$. It is worth noting that for g_a or $g_b = 0$, the system reduces to a model of small atoms coupling to a TW.

III. TOPOLOGY-DEPENDENT GIANT-ATOM–PHOTON BOUND STATES

In this section we discuss the giant-atom–photon bound states in the single-excitation subspace. We consider that a giant atom couples to the TW at the mth cell and the $(m + l)$th cell. The bound state of the wave function has the form

$$|\psi_{\rm BS}\rangle = \left(C_e \sigma^\dagger + \sum_k \left(C_k^\alpha \alpha_k^\dagger + C_k^\beta \beta_k^\dagger\right)\right)|g, \text{vac}\rangle, \quad (8)$$

where C_σ and $C_k^{\alpha(\beta)}$ are the probability amplitudes for giant atom and photons, respectively. By solving the Schrödinger equation $H|\psi_{\rm BS}\rangle = E_{\rm BS}|\psi_{\rm BS}\rangle$ with $E_{\rm BS}$ lying outside the bands, we can obtain the probability amplitudes of photons under the diagonalized basis

$$C_k^\beta = \frac{1}{\sqrt{N}} \frac{C_e q(k) e^{-ikx_m}}{E_{\rm BS} + \omega(k)},$$
$$C_k^\alpha = \frac{1}{\sqrt{N}} \frac{C_e p(k) e^{-ikx_m}}{E_{\rm BS} - \omega(k)}. \quad (9)$$

In addition, the eigenenergy satisfies the transcendental equation

$$E_{\rm BS} = \Delta + \int_{-\pi}^{\pi} \frac{dk}{2\pi} \left(\frac{|p(k)|^2}{E_{\rm BS} - \omega(k)} + \frac{|q(k)|^2}{E_{\rm BS} + \omega(k)}\right). \quad (10)$$

It is difficult to obtain an analytical solution of the transcendental equation. Instead, we can appeal to the numerical diagonalization of the Hamiltonian in real space and plot the energy spectrum in single excitation under periodic boundary conditions. In Fig. 2(b) we plot the energy spectrum varying with Δ. The energy levels marked in blue are the scattering states and those marked in red are the bound states [52]. It can be seen that in each band gap there exists a bound state such as the points P_1, P_2, and P_3. Thus, for a given Δ, we can obtain the energy of the bound state $E_{\rm BS}$ on the energy spectrum.

Combining with the relationship between (α_k, β_k) and (a_k, b_k), we can find that the probability amplitudes for photons $C_k^{a(b)}$ satisfy

$$C_k^a = \frac{C_e}{\sqrt{N}} \frac{[g_a E_{\rm BS} + g_b \omega(k) e^{i[\phi(k) - kl]}] e^{-ikx_m}}{E_{\rm BS}^2 - \omega(k)^2},$$
$$C_k^b = \frac{C_e}{\sqrt{N}} \frac{[g_b E_{\rm BS} e^{-ikl} + g_a \omega(k) e^{-i\phi(k)}] e^{-ikx_m}}{E_{\rm BS}^2 - \omega(k)^2}. \quad (11)$$

Transferring the probability amplitudes in momentum space to real space by a Fourier transform, we can obtain the probability amplitudes $C_j^{a(b)}$ in the real space.

In Fig. 3 we plot the probability distribution $|C_j^{a(b)}|^2$ on the cells by numerically calculating Eq. (11), where we choose detuning values corresponding to the three points in Fig. 2(b), i.e., $\Delta = -2.3J$ (P_1), 0 (P_2), and $2.3J$ (P_3), with the bound-state energies $E_{\rm BS} = -2.317J$, 0, and $2.317J$, respectively.

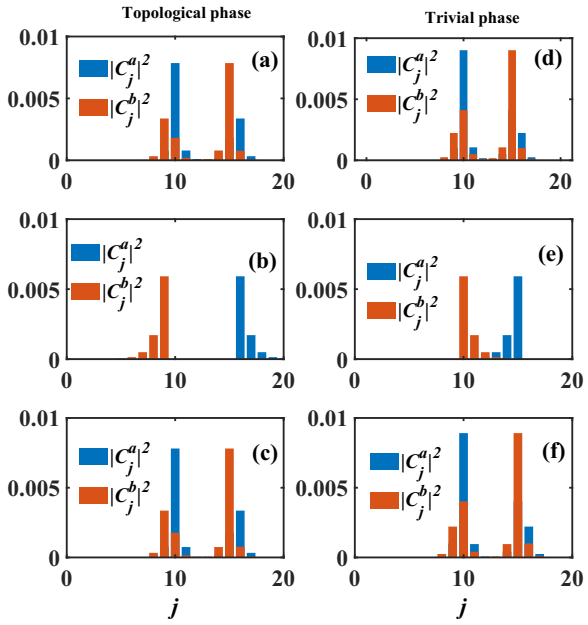

FIG. 3. Probability distributions of the photon bound states $|C_j^a|^2$ and $|C_j^b|^2$ for (a) and (d) $\Delta = 2.3J$, (b) and (e) $\Delta = 0$, (c) and (f) $\Delta = -2.3J$ for the waveguide in (a)–(c) the topological phase ($\delta = 0.3$) and (d)–(f) the trivial phase ($\delta = -0.3$). The other parameters are $g_a = g_b = 0.1$, $m = 10$, $l = 5$, and $N = 20$.

Figures 3(a)–3(c) correspond to the waveguide in the topological phase ($\delta = 0.3$) and Figs. 3(d)–3(f) correspond to the waveguide in the trivial phase ($\delta = -0.3$). For the giant atom the frequency falls in the upper band gap with $\Delta = 2.3J$, as shown in Figs. 3(a) and 3(d); the photon probability distributions are similar, with $\Delta = -2.3J$ shown in Figs. 3(c) and 3(f), and are mainly distributed in the sublattices A and B near the giant-atom coupling node. Then the topological properties of the waveguide have no particular effect on the distribution of bound states for $\Delta = \pm 2.3J$.

However, for the giant atom the frequency falls in the middle band gap with $\Delta = 0$, as displayed in Figs. 3(b) and 3(e), although also mostly distributed near the giant-atom coupling nodes, the photons are distinctly different from $\Delta = \pm 2.3J$. Specifically, when the TW is in the topological phase, the photons are distributed only on the left sublattice B of the left coupling node and on the right sublattice A of the second coupling node, and photons are not distributed within the giant atom. When the TW is in the trivial phase, the photons are distributed only on the right sublattice B of the left coupling node and on the left sublattice A of the second coupling node. Consequently, they are only distributed within the giant atom. Overall, the topology of the waveguide has a completely different effect on the giant-atom photon bound state for $\Delta = 0$. When multiple small atoms are coupled within a band gap in a structured waveguide, effective dipole-dipole interactions between them through the exchange of virtual photons and the strength of the interactions depend on the overlap between bound states [50,53–55]. The case is also valid for giant atoms, where interactions between giant atoms can be mediated when photon wave functions around different giant atoms are overlapped together. In particular, for $\Delta = 0$, since the

distribution of photons in the topological phase is significantly different from that in the trivial phase, the dipole interactions between the giant atoms exhibit topology-dependent exotic phenomena when multiple giant atoms are coupled to the TW at the band gap, as we discuss in the next section.

IV. VIRTUAL-PHOTON-INDUCED INTERACTIONS BETWEEN GIANT ATOMS

The overlap of the wave function between the bound states of the multiple giant atoms induces coherent interaction between giant atoms, and the coherent interaction can be described with an effective Hamiltonian by eliminating the waveguide mode [50,51]. Next we derive the effective Hamiltonian between giant atoms. By employing the large detuning method, under the diagonal basis vector, the full Hamiltonian is

$$H = H_0 + H_I, \tag{12}$$

with

$$H_0 = \sum_k \omega(k)(\alpha_k^\dagger \alpha_k - \beta_k^\dagger \beta_k) + \sum_{n=1}^{M} \omega_o \sigma_n^\dagger \sigma_n,$$
$$H_I = \frac{1}{\sqrt{N}} \sum_{n=1}^{M} \sum_k \{e^{-ikx_n}[p(k)\alpha_k^\dagger + q(k)\beta_k^\dagger]\sigma_n + \text{H.c.}\}. \tag{13}$$

We use the Schrieffer-Wolff transformation to adiabatically eliminate the photon modes [56]. Define $S = \sum_k [-(\eta_{\alpha,k}\alpha_k + \zeta_{\beta,k}\beta_k)\sigma_n^\dagger + (\eta_{\alpha,k}^* \alpha_k^\dagger + \zeta_{\beta,k}^* \beta_k^\dagger)\sigma_n]$, where S is an anti-Hermitian operator $S^\dagger = -S$. Then the Hamiltonian becomes

$$H_S = UHU^\dagger = H + [S, H] + \tfrac{1}{2}[S, [S, H]] + \cdots, \tag{14}$$

where $U = e^S$. By setting the term of the first-order perturbation to zero as $H_I + [H_0, S] = 0$, we can find that the determined parameters satisfies $\eta_{\alpha,k} = \frac{p(k)e^{-ikx_n}}{\sqrt{N}[\Delta - \omega(k)]}$ and $\zeta_{\beta,k} = \frac{q(k)e^{-ikx_n}}{\sqrt{N}[\Delta + \omega(k)]}$. In the case of $\{\eta_{\alpha,k}, \zeta_{\beta,k}\} \ll 1$, we can keep only the second-order terms and safely omit the higher-order terms. This is equivalent to the large detuning condition as $\{g_a, g_b\} \ll N|\Delta - \Delta_{\text{edge}}|$, where Δ_{edge} is the band edge as $\{-2J, -2J\delta, 2J\delta, 2J\}$, which is the specific requirement for $(g_a, g_b) \ll (J_1, J_2)$. The large detuning condition seems a mathematical requirement. Actually, the weak-coupling approximation is also a physical requirement for achieving atomic interactions mediated by a waveguide. The excitation of photons is equal to dissipation for the atom interaction; then the virtual excitation of photons favors our goal. Therefore, the weak coupling is necessary because under this condition excitation of photons is nearly virtual. Then, under the second-order perturbation approximation, we can obtain

$$H_S = \sum_{n,m} (J_{nm}\sigma_n^\dagger \sigma_m + \text{H.c.}), \tag{15}$$

with $J_{nm} = \sum_k \frac{1}{N}(\frac{|p(k)|^2}{\Delta - \omega(k)} + \frac{|q(k)|^2}{\Delta + \omega(k)})e^{ikx_{nm}}$, where $x_{nm} = x_m - x_n$ refers to the distance between giant atoms, namely, the distance between the cavities corresponding to the first coupling nodes of different giant atoms. By replacing the discrete modes with the continuous distribution, we can obtain

$$J_{nm} = \int_{-\pi}^{\pi} \frac{dk}{2\pi} \left(\frac{|p(k)|^2}{\Delta - \omega(k)} + \frac{|q(k)|^2}{\Delta + \omega(k)} \right) e^{ikx_{nm}}. \tag{16}$$

Bringing the parameters $p(k)$, $q(k)$, and $\omega(k)$ into the integral, we can numerically obtain the interactions between giant atoms. In particular, for $\Delta = 0$ we can analytically obtain the effective interaction for the TW in the topological phase

$$J_{nm} = \begin{cases} 0, & l - x_{nm} + 1 > 0 \\ -\frac{g_a g_b}{J_1}(-\frac{J_1}{J_2})^{x_{nm}-l}, & l - x_{nm} + 1 \leqslant 0 \end{cases} \tag{17}$$

and in the trivial phase

$$J_{nm} = \begin{cases} -\frac{g_a g_b}{J_1}(-\frac{J_1}{J_2})^{x_{nm}-l}, & l - x_{nm} + 1 > 0 \\ 0, & l - x_{nm} + 1 \leqslant 0. \end{cases} \tag{18}$$

From Eqs. (17) and (18) we can see that the interactions between the giant atoms depend on the topology of the waveguide and the difference between x_{nm} and l. For example, for a TW in the topological phase, when the distance between two coupling points of a single giant atom is longer than the distance between two giant atoms ($l > x_{nm}$), the two giant atoms are bridged and there is no interaction between them. The interaction exists only when $l < x_{nm}$, namely, the two giant atoms are separated. In addition, for fixed δ, the coupling is invariant as long as $x_{nm} - l$ is invariant. Thus, the interaction between giant atoms depends on $x_{nm} - l$.

In Fig. 4 we plot the coherent interaction between giant atoms $|J_{nm}|$ varying with x_{nm} for different l, Δ, and δ. For the frequency of giant atoms lying in the upper band of the TW, with $\Delta = 2.3J$ and $\delta = 0.3$ shown in Fig. 4(a), we can see that when $l = 0$, the effective interaction between giant atoms decreases with increasing x_{nm}. For $l \neq 0$, when $x_{nm} < l$ (two

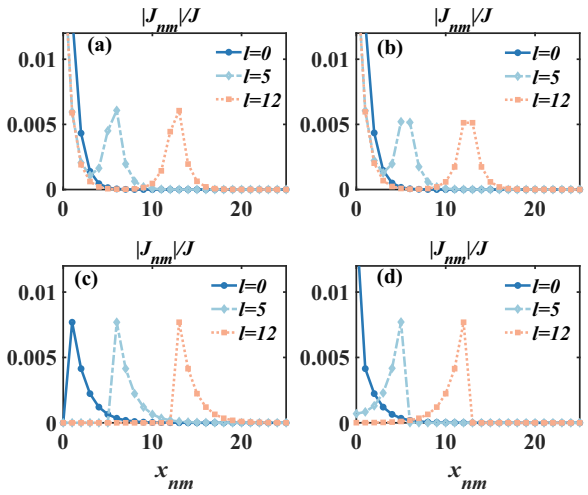

FIG. 4. (a) Variation of the coherent interaction between giant atoms $|J_{nm}|$ with x_{nm} (dimensionless) for $l = 0, 5, 10$ with (a) $\Delta = 2.3J$ and $\delta = 0.3$, (b) $\Delta = 2.3J$ and $\delta = 0$, (c) $\Delta = 0$ and $\delta = 0.3$, and (d) $\Delta = 0$ and $\delta = -0.3$. The other parameters are $g_a = g_b = 0.1J$.

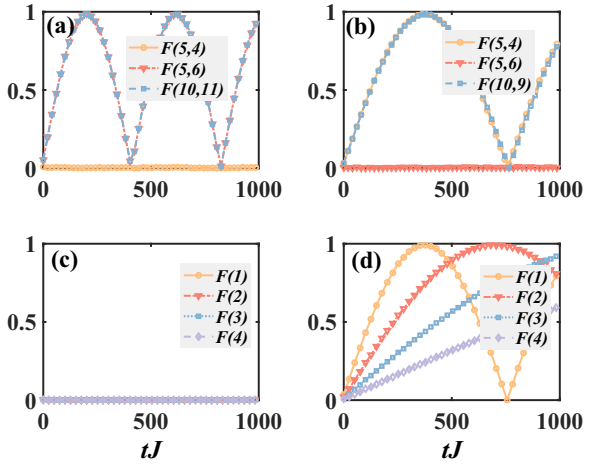

FIG. 5. Dynamic evolution of fidelity $F(l, x_{nm})$ governed by Eq. (1) for (a) $\delta = 0.3$ and (b) $\delta = -0.3$. The small-atom excitation transfer fidelity $F(x_{nm})$ varies with t for (c) $\delta = 0.3$ and (d) $\delta = -0.3$. The other parameters are $g_a = g_b = 0.1J$, $\Delta = 0$, and $N = 40$.

giant atoms are separated), the effective interactions show a U-shaped configuration; when $x_{nm} > l$ (two giant atoms are bridged), the effective interaction decreases with increasing x_{nm}, while the maximum value of the interaction corresponds to $x_{nm} = l + 1$ for different l. For $\Delta = 2.3J$ and $\delta = 0$, as shown in Fig. 4(b), the effective interaction between giant atoms varies with x_{nm} as in Fig. 4(a). However, when the giant atom frequency falls in the middle band gap with $\Delta = 0$, by comparing Figs. 4(c) and 4(d) we can see that the effective interactions between giant atoms exhibit topology-dependent behavior. Specifically, for $l = 0$, the energy shift of the single giant atom $\Delta_s = J_{nn}$ corresponding to $x_{nm} = 0$ for the TW in the topological phase ($\delta = 0.3$) is zero $\Delta_s = 0$ and in the TW trivial phase ($\delta = -0.3$) the energy shifted becomes $\Delta_s = -g_a g_b / J_1$. For $l \neq 0$ and the TW in the topological phase, when $l > x_{nm}$ there is no interaction between the giant atoms, while when $l < x_{nm}$ (the two giant atoms are bridged) the interaction between the giant atoms decreases with distance. The maximum value of the interaction is constant with respect to $x_{nm} = l + 1$ under different l as displayed in Fig. 4(c), which means that we can realize coupling between two distant giant atoms only with $l < x_{nm}$. In the TW in the trivial phase shown in Fig. 4(d), the results are completely opposite to that in the topological phase, where the interaction between giant atoms increases with the distance between them when $l > x_{nm}$ and the maximum value of the interaction is constant with respect to $x_{nm} = l$ under different l for $l \neq 0$, while the interaction between two giant atoms disappears when $l < x_{nm}$. For the TW in the topological phase ($\delta = 0.3$) and trivial phase ($\delta = -0.3$), the reason for the different interactions is caused by the different distribution of photon bound states for the two cases (see Fig. 3). For the TW in the topological phase with $\Delta = 0$, the photons are distributed only on the outside of the giant atoms. When $x_{nm} < l$, photon bound states around the giant atoms do not overlap and therefore do not induce interactions between them; it is only when $x_{nm} > l$ that photon bound states overlap and then the interaction between giant atoms can exist. Meanwhile, when the distance between atoms increases, the degree of overlapping of the photon wave functions decreases, which results in the decrease of interactions. In other words, for $l \neq 0$, when $\Delta = 0$, the interactions exhibit topological dependence. When the TW is in the topological phase, there is no interaction for $x_{nm} < l$; only when $x_{nm} > l$ is the effective interaction induced, which can offer us a method to realize a double chain. When the TW is in the trivial phase, only if $x_{nm} < l$ do the giant atoms interact with each other, which provides us a method to model chains of giant atoms with only nearest-neighbor interactions.

Next we would like to prove the topology-dependent effective interaction between the two giant atoms using the full Hamiltonian (1). We employ fidelity F to indicate the effective exchange interaction by transferring the excitation from the left giant atom to the right giant atom. The fidelity is defined as $F(l, x_{nm}) = \langle \psi_t | \psi_f \rangle$, with $|\psi_f\rangle$ ($|\psi_t\rangle$) the wave function of the final (target) state. We assume that initially the left giant atom is in the excited state and the right giant atom is in the ground state. The fidelity equal to 1 means that the excitation is transferred from the left giant atom to the right one. In Figs. 5(a) and 5(b) we plot the fidelity $F(l, x_{nm})$ varying with t for $\Delta = 0$ and $\delta = \pm 0.3$. When the TW is in the topological phase ($\delta = 0.3$) [see Fig. 5(a)], $F(l, x_{nm})$ is always zero when $l > x_{nm}$, which implies there is no effective interaction between them, which is consistent with Fig. 4(c). Meanwhile, when $l < x_{nm}$, we can see that $F(l, x_{nm})$ is periodically varying, where the period of fidelity evolution can indicate the effective interaction between giant atoms. For the TW in the trivial phase ($\delta = -0.3$), as displayed in Fig. 5(b), we can see that the result is opposite that in the topological phase, where $F(l, x_{nm})$ is periodically varying when $l > x_{nm}$, while $F(l, x_{nm})$ is always zero for $l < x_{nm}$. Interestingly, the evolution of $F(12, 13)$ is consistent with that of $F(5, 6)$ when $\delta = 0.3$ and that of $F(12, 11)$ is consistent with that of $F(5, 4)$ when $\delta = -0.3$, which proves that the effective coupling depends only on the difference between x_{nm} and l, which is consistent with Figs. 4(c) and 4(d). Thus, by analyzing the behavior of the transfer fidelity of the giant-atom excitations under the full Hamiltonian, we can predict from the dynamics of the process that the topology-dependent interactions are reasonable.

In order to see the characteristics of the current system, in Fig. 5(c) we plot the time evolution of the fidelity $F(x_{nm})$ for the case of small atoms coupling to a TW so as to compare the difference between giant atoms and small atoms. We can see that in the topological phase the excitation cannot be transferred. For $\delta = -0.3$ [see Fig. 5(d)] the period of fidelity $F(x_{nm})$ increases with increasing distance. The minimum fidelity period corresponds to $x_{nm} = 1$. Only when the TW is in the trivial phase can the excitation transfer between the two small atoms occur, which is consistent with [37]. Comparing Figs. 5(a)–5(d), we can see that the minimum periods of the small and giant atoms are almost the same for a TW in the trivial phase and both are smaller than the giant-atom coupled to a TW in the topological phase. Overall, compared to small atoms, giant atoms can realize excitation transfer in any topology of the TW.

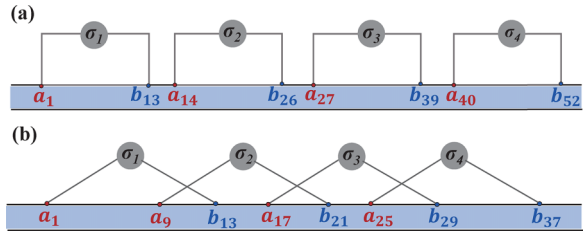

FIG. 6. Schematic diagram of a coupled waveguide with multiple giant atoms. (a) Neighboring giant atoms are separated from each other for $l < x_{nm}$. (b) Neighboring giant atoms are bridged to each other for $l > x_{nm}$. The coupling strengths of the giant atoms coupled to the TW are all g_a and the detuning of all giant atoms is set to $\Delta = 0$.

V. SIMULATION OF NEAREST-NEIGHBOR INTERACTIONS AND the DOUBLE-CHAIN STRUCTURE OF GIANT-ATOM CHAINS

In this section we use this topology-dependent interaction to simulate pure nearest-neighbor interaction models as well as double-chain structure models. We consider two configurations of giant-atom chain structures, where the distance between two coupling nodes of a single giant atom is $l = 12$. As shown in Fig. 6(a), the giant atoms are coupled to the topological chain separately from each other. The distance between neighboring giant atoms is $x_{n,n+1} = 13$. Because the distance between atoms in the next-nearest neighbor is greater than $x_{n,n+2} = 26$, the induced interactions are almost zero, as displayed in Fig. 4(c); therefore, there are no next-nearest-neighbor interactions between giant atoms. In this case, the effective Hamiltonian of the giant-atom chain can be written in the spin picture as

$$H_{\text{chain}} = \sum_{n=1}^{M} \frac{2g_a^2}{J_2}\left(\sigma_n^x \sigma_{n+1}^x + \sigma_n^y \sigma_{n+1}^y\right). \tag{19}$$

It can be seen that the Hamiltonian (19) describes a one-dimensional spin-1/2 chain with XX-type nearest-neighbor coupling. The model is widely used in quantum communication [57] and quantum information processing [58,59].

For the second configuration as shown in Fig. 6(b), we consider the nearest-neighbor giant atoms to be bridged and separated from next-nearest-neighbor giant atoms. The distance between neighboring giant atoms is $x_{n,n+1} = 8$. For the TW in the trivial phase, according to Eq. (18), we can derive the effective interaction Hamiltonian for the chain of giant atoms to be the same as in Eq. (19) except that the coupling becomes $-\frac{g_a^2}{J_1}(-\frac{J_2}{J_1})^4$. For the TW in the topological phase, according to Eq. (17), we can derive the effective interaction Hamiltonian for the chain of giant atoms as

$$H_{\text{chain}} = T\sum_{n=1}^{M}(\sigma_{2n-1}^{\dagger}\sigma_{2n+1} + \sigma_{2n}^{\dagger}\sigma_{2n+2} + \text{H.c.}), \tag{20}$$

where $T = -\frac{g_a^2 J_1^3}{J_2^4}$. This Hamiltonian describes a double-chain model, where one chain represents coupling between odd-numbered giant atoms and the other between even-numbered giant atoms. For example, for $M = 4$ (four giant atoms), the Hamiltonian (20) becomes $H_{\text{chain}} = -\frac{g_a^2 J_1^3}{J_2^4}(\sigma_1^{\dagger}\sigma_3 + \sigma_2^{\dagger}\sigma_4 + \text{H.c.})$. For the initial state $|\psi(0)\rangle = \{1;0;0;0\}$, where the first giant atom is in the excited state and the other giant atom is in the ground state, under the Hamiltonian H_{chain}, the final state will evolve as $|\psi(t)\rangle = \{\cos(Tt);0;\sin(Tt);0\}$. Choosing the evolution time $t_f = \pi/4T$, we can realize the maximally entangled state between the first and third giant atoms $|\psi(t_f)\rangle = \{1/\sqrt{2};0;1/\sqrt{2};0\}$. In the same way, we can achieve the maximally entangled state of the second and fourth giant atoms. In addition, if the initial state of the system is assumed to be in an arbitrary entangled state of the first and second giant atoms $|\psi(0)\rangle = \{\sqrt{p};\sqrt{1-p};0;0\}$, then at evolution time $t_f = \pi/4T$, the final state becomes $|\psi(t_f)\rangle = \{0;0;\sqrt{p};\sqrt{1-p}\}$, which is an arbitrary entangled state of the third and fourth giant atoms. Thus, the structure of the double chain can be used not only to prepare a maximally entangled state of two giant atoms but also to transfer an arbitrary entangled state.

VI. DISCUSSION AND CONCLUSION

It should be noted that giant atoms coupling to topological waveguides has not been reported experimentally. The coupling of giant atoms to waveguides [60] and the coupling of small atoms to topological waveguides [34] have been realized recently in superconducting circuits. The parameters used in this paper, for example, the coupling strength between neighboring microwave cavities $J = 256$ MHz [34] and the coupling strength between giant atoms and the waveguide $g_a = 0.01J = 2.56$ MHz, are within the experimental range that has been realized in experiment [60]. Therefore, our proposed model may theoretically be promising for implementation in superconducting circuits.

In this paper we considered the topological effects on the giant-atom–photon bound states in the giant-atom coupled TW system and showed that the spatial distribution of the giant-atom–photon bound states exhibits a clear topological dependence. When multiple small atoms are coupled within the band gap of the TW, the effective dipole-dipole interactions are generated between the giant atoms by exchanging virtual photons, and the strength of the interactions depends on the degree of overlap between the bound states. Thus, topologically dependent bound states can be induced by topologically dependent dipole-dipole interactions between giant atoms. Employing this feature, we considered two configurations of giant-atom chain structures and found that they lead to the purely nearest-neighbor interaction and double independent next-nearest-neighbor interactions between giant atoms. Furthermore, we found that the structure of the double chain can be used not only to prepare a maximally entangled state of two giant atoms but also to transfer an arbitrary entangled state.

ACKNOWLEDGMENTS

This work was supported by the National Natural Science Foundation of China under Grants No. 12274053 and No. 12375010.

[1] A. S. Sheremet, M. I. Petrov, I. V. Iorsh, A. V. Poshakinskiy, and A. N. Poddubny, Waveguide quantum electrodynamics: collective radiance and photon-photon correlations, Rev. Mod. Phys. **95**, 015002 (2023).

[2] A. Blais, A. L. Grimsmo, S. M. Girvin, and A. Wallraff, Circuit quantum electrodynamics, Rev. Mod. Phys. **93**, 025005 (2021).

[3] M. O. Scully and M. S. Zubairy, *Quantum Optics* (Cambridge University Press, Cambridge, 1997).

[4] B. Kannan, M. J. Ruckriegel, D. L. Campbell, A. Frisk Kockum, J. Braumüller, D. K. Kim, M. Kjaergaard, P. Krantz, A. Melville, B. M. Niedzielski, A. Vepsäläinen, R. Winik, J. L. Yoder, F. Nori, T. P. Orlando, S. Gustavsson, and W. D. Oliver, Waveguide quantum electrodynamics with superconducting artificial giant atoms, Nature (London) **583**, 775 (2020).

[5] G. Andersson, B. Suri, L. Guo, T. Aref, and P. Delsing, Non-exponential decay of a giant artificial atom, Nat. Phys. **15**, 1123 (2019).

[6] G. Andersson, M. K. Ekström, and P. Delsing, Electromagnetically induced acoustic transparency with a superconducting circuit, Phys. Rev. Lett. **124**, 240402 (2020).

[7] C. Joshi, F. Yang, and M. Mirhosseini, Resonance fluorescence of a chiral artificial atom, Phys. Rev. X **13**, 021039 (2023).

[8] A. González-Tudela, C. S. Muñoz, and J. I. Cirac, Engineering and harnessing giant atoms in high-dimensional baths: A proposal for implementation with cold atoms, Phys. Rev. Lett. **122**, 203603 (2019).

[9] N. Gheeraert, S. Kono, and Y. Nakamura, Programmable directional emitter and receiver of itinerant microwave photons in a waveguide, Phys. Rev. A **102**, 053720 (2020).

[10] J. Zhou, X.-L. Yin, and J.-Q. Liao, Chiral and nonreciprocal single-photon scattering in a chiral-giant-molecule waveguide-QED system, Phys. Rev. A **107**, 063703 (2023).

[11] Z. Q. Wang, Y. P. Wang, J. Yao, R. C. Shen, W. J. Wu, J. Qian, J. Li, S. Y. Zhu, and J. Q. You, Giant spin ensembles in waveguide magnonics, Nat. Commun. **13**, 7508 (2022).

[12] X. Wang, Q.-Y. Qiu, K.-W. Huang, and H. Xiong, Nonreciprocal single-photon scattering in giant-spin-ensemble–waveguide magnonics, Phys. Rev. A **108**, 063715 (2023).

[13] A. Frisk Kockum, P. Delsing, and G. Johansson, Designing frequency-dependent relaxation rates and Lamb shifts for a giant artificial atom, Phys. Rev. A **90**, 013837 (2014).

[14] A. F. Kockum, G. Johansson, and F. Nori, Decoherence-free interaction between giant atoms in waveguide quantum electrodynamics, Phys. Rev. Lett. **120**, 140404 (2018).

[15] A. Soro, C. S. Muñoz, and A. F. Kockum, Interaction between giant atoms in a one-dimensional structured environment, Phys. Rev. A **107**, 013710 (2023).

[16] L. Du, L. Guo, and Y. Li, Complex decoherence-free interactions between giant atoms, Phys. Rev. A **107**, 023705 (2023).

[17] A. Soro and A. F. Kockum, Chiral quantum optics with giant atoms, Phys. Rev. A **105**, 023712 (2022).

[18] X. Wang, T. Liu, A. F. Kockum, H.-R. Li, and F. Nori, Tunable chiral bound states with giant atoms, Phys. Rev. Lett. **126**, 043602 (2021).

[19] L. Du, Y.-T. Chen, and Y. Li, Nonreciprocal frequency conversion with chiral Λ-type atoms, Phys. Rev. Res. **3**, 043226 (2021).

[20] L. Du, M.-R. Cai, J.-H. Wu, Z. Wang, and Y. Li, Single-photon nonreciprocal excitation transfer with non-Markovian retarded effects, Phys. Rev. A **103**, 053701 (2021).

[21] A. C. Santos and R. Bachelard, Generation of maximally entangled long-lived states with giant atoms in a waveguide, Phys. Rev. Lett. **130**, 053601 (2023).

[22] X.-L. Yin and J.-Q. Liao, Generation of two-giant-atom entanglement in waveguide-QED systems, Phys. Rev. A **108**, 023728 (2023).

[23] L. Guo, A. F. Kockum, F. Marquardt, and G. Johansson, Oscillating bound states for a giant atom, Phys. Rev. Res. **2**, 043014 (2020).

[24] K. H. Lim, W.-K. Mok, and L.-C. Kwek, Oscillating bound states in non-Markovian photonic lattices, Phys. Rev. A **107**, 023716 (2023).

[25] S. Guo, Y. Wang, T. Purdy, and J. Taylor, Beyond spontaneous emission: Giant atom bounded in the continuum, Phys. Rev. A **102**, 033706 (2020).

[26] X. Zhang, C. Liu, Z. Gong, and Z. Wang, Quantum interference and controllable magic cavity qed via a giant atom in a coupled resonator waveguide, Phys. Rev. A **108**, 013704 (2023).

[27] X.-L. Yin, W.-B. Luo, and J.-Q. Liao, Non-Markovian disentanglement dynamics in double-giant-atom waveguide-QED systems, Phys. Rev. A **106**, 063703 (2022).

[28] Y. T. Zhu, S. Xue, R. B. Wu, W. L. Li, Z. H. Peng, and M. Jiang, Spatial-nonlocality-induced non-Markovian electromagnetically induced transparency in a single giant atom, Phys. Rev. A **106**, 043710 (2022).

[29] T. Ozawa, H. M. Price, A. Amo, N. Goldman, M. Hafezi, L. Lu, M. C. Rechtsman, D. Schuster, J. Simon, O. Zilberberg, and I. Carusotto, Topological photonics, Rev. Mod. Phys. **91**, 015006 (2019).

[30] M. Z. Hasan and C. L. Kane, *Colloquium:* Topological insulators, Rev. Mod. Phys. **82**, 3045 (2010).

[31] M. I. Shalaev, W. Walasik, A. Tsukernik, Y. Xu, and N. M. Litchinitser, Robust topologically protected transport in photonic crystals at telecommunication wavelengths, Nat. Nanotechnol. **14**, 31 (2019).

[32] L. A. Wray, S. Y. Xu, Y. Xia, Y. S. Hor, D. Qian, A. V. Fedorov, H. Lin, A. Bansil, R. J. Cava, and M. Z. Hasan, Observation of topological order in a superconducting doped topological insulator, Nat. Phys. **6**, 855 (2010).

[33] X. Zhang, E. Kim, D. K. Mark, S. Choi, and O. Painter, A superconducting quantum simulator based on a photonic-bandgap metamaterial, Science **379**, 278 (2023).

[34] E. Kim, X. Zhang, V. S. Ferreira, J. Banker, J. K. Iverson, A. Sipahigil, M. Bello, A. González-Tudela, M. Mirhosseini, and O. Painter, Quantum electrodynamics in a topological waveguide, Phys. Rev. X **11**, 011015 (2021).

[35] A. Blanco-Redondo, I. Andonegui, M. J. Collins, G. Harari, Y. Lumer, M. C. Rechtsman, B. J. Eggleton, and M. Segev, Topological optical waveguiding in silicon and the transition between topological and trivial defect states, Phys. Rev. Lett. **116**, 163901 (2016).

[36] L.-C. Wang, Y. Chen, M. Gong, F. Yu, Q.-D. Chen, Z.-N. Tian, X.-F. Ren, and H.-B. Sun, Edge state, localization length, and critical exponent from survival probability in topological waveguides, Phys. Rev. Lett. **129**, 173601 (2022).

[37] M. Bello, G. Platero, J. I. Cirac, and A. González-Tudela, Unconventional quantum optics in topological waveguide QED, Sci. Adv. **5**, eaaw0297 (2019).

[38] L. Leonforte, A. Carollo, and F. Ciccarello, Vacancy-like dressed states in topological waveguide QED, Phys. Rev. Lett. **126**, 063601 (2021).

[39] M. Bello, G. Platero, and A. González-Tudela, Spin many-body phases in standard- and topological-waveguide QED simulators, PRX Quantum **3**, 010336 (2022).

[40] C. Vega, M. Bello, D. Porras, and A. González-Tudela, Qubit-photon bound states in topological waveguides with long-range hoppings, Phys. Rev. A **104**, 053522 (2021).

[41] W. Cheng, Z. Wang, and Y.-X. Liu, Topology and retardation effect of a giant atom in a topological waveguide, Phys. Rev. A **106**, 033522 (2022).

[42] X. Wang, Z.-M. Gao, J.-Q. Li, H.-B. Zhu, and H.-R. Li, Unconventional quantum electrodynamics with a Hofstadter-ladder waveguide, Phys. Rev. A **106**, 043703 (2022).

[43] C. Vega, D. Porras, and A. González-Tudela, Topological multimode waveguide QED, Phys. Rev. Res. **5**, 023031 (2023).

[44] R. Bag and D. Roy, Quantum light-matter interactions in structured waveguides, Phys. Rev. A **108**, 053717 (2023).

[45] X.-L. Dong, C.-P. Shen, S.-Y. Gao, H.-R. Li, H. Gao, F.-L. Li, and P.-B. Li, Chiral spin-phonon bound states and spin-spin interactions with phononic lattices, Phys. Rev. Res. **4**, 023077 (2022).

[46] W. Nie, Z. H. Peng, F. Nori, and Y.-X. Liu, Topologically protected quantum coherence in a superatom, Phys. Rev. Lett. **124**, 023603 (2020).

[47] W. Nie, T. Shi, F. Nori, and Y.-X. Liu, Topology-enhanced nonreciprocal scattering and photon absorption in a waveguide, Phys. Rev. Appl. **15**, 044041 (2021).

[48] X. Z. Hao, X. Y. Zhang, Y. H. Zhou, C. M. Dai, S. C. Hou, and X. X. Yi, Topologically protected optomechanically induced transparency in a one-dimensional optomechanical array, Phys. Rev. A **105**, 013505 (2022).

[49] G. Calajó, F. Ciccarello, D. Chang, and P. Rabl, Atom-field dressed states in slow-light waveguide QED, Phys. Rev. A **93**, 033833 (2016).

[50] J. S. Douglas, H. Habibian, C. L. Hung, A. V. Gorshkov, H. J. Kimble, and D. E. Chang, Quantum many-body models with cold atoms coupled to photonic crystals, Nat. Photon. **9**, 326 (2015).

[51] M. Scigliuzzo, G. Calajò, F. Ciccarello, D. Perez Lozano, A. Bengtsson, P. Scarlino, A. Wallraff, D. Chang, P. Delsing, and S. Gasparinetti, Controlling atom-photon bound states in an array of Josephson-junction resonators, Phys. Rev. X **12**, 031036 (2022).

[52] W. Zhao and Z. Wang, Single-photon scattering and bound states in an atom-waveguide system with two or multiple coupling points, Phys. Rev. A **101**, 053855 (2020).

[53] S. John and J. Wang, Quantum optics of localized light in a photonic band gap, Phys. Rev. B **43**, 12772 (1991).

[54] C.-L. Hung, S. M. Meenehan, D. E. Chang, O. Painter, and H. J. Kimble, Trapped atoms in one-dimensional photonic crystals, New J. Phys. **15**, 083026 (2013).

[55] A. González-Tudela, C. L. Hung, D. E. Chang, J. I. Cirac, and H. J. Kimble, Subwavelength vacuum lattices and atom-atom interactions in two-dimensional photonic crystals, Nat. Photon. **9**, 320 (2015).

[56] J. R. Schrieffer and P. A. Wolff, Relation between the Anderson and Kondo Hamiltonians, Phys. Rev. **149**, 491 (1966).

[57] T. J. G. Apollaro, G. M. A. Almeida, S. Lorenzo, A. Ferraro, and S. Paganelli, Spin chains for two-qubit teleportation, Phys. Rev. A **100**, 052308 (2019).

[58] F. Benatti, R. Floreanini, and L. Memarzadeh, Exact steady state of the open XX-spin chain: Entanglement and transport properties, PRX Quantum **2**, 030344 (2021).

[59] A. Imamoğlu, D. D. Awschalom, G. Burkard, D. P. DiVincenzo, D. Loss, M. Sherwin, and A. Small, Quantum information processing using quantum dot spins and cavity QED, Phys. Rev. Lett. **83**, 4204 (1999).

[60] M. Mirhosseini, E. Kim, V. S. Ferreira, M. Kalaee, A. Sipahigil, A. J. Keller, and O. Painter, Superconducting metamaterials for waveguide quantum electrodynamics, Nat. Commun. **9**, 3706 (2018).